Journal of Molecular Modeling (2023) 29:222
https://doi.org/10.1007/s00894-023-05636-y

ORIGINAL PAPER

Aqueous degradation of 6-APA by hydroxyl radical: a theoretical study

Seyda Aydogdu[1] · **Arzu Hatipoglu**[1]

Received: 30 March 2023 / Accepted: 26 June 2023 / Published online: 3 July 2023

Abstract

Context Degradation reactions of micropollutants such as antibiotics with OH radicals are very important in terms of environmental pollution. Therefore, in this study, the degradation kinetic mechanism of 6-aminopenicillanic acid (6-APA) with OH radical was investigated by density functional theory (DFT) methods.

Methods For the calculations, different functionals such as B3LYP, MPW1PW91, and M06-2X were used with a 6-31 g(d,p) basis set. The aquatic effect on the reaction mechanism was investigated by conductor-like polarizable continuum model (CPCM). For the degradation kinetics in aqueous media, the addition of explicit water molecules was also calculated. Subsequent reaction mechanism for the most probable reaction product was briefly discussed.

Results Among the functionals used, B3LYP results were consistent with the experimental results. Calculated kinetic parameters indicated that the OH-addition path was more dominant than the H-abstraction paths. With the increase of explicit water molecules in the models, the energy required for the formation of transition state complexes decreased. The overall rate constant is calculated as 2.28×10^{11} M^{-1} s^{-1} at 298 K for the titled reaction.

Keywords 6-Aminopenicillanic acid · Density functional theory · Hydroxyl radical · Kinetics

Introduction

Approximately 210,000 tons of antibiotics are produced all over the world every year, and beta-lactam antibiotics are the most consumed ones [1, 2]. 6-Aminopenicillanic acid (6-APA) is a beta-lactam-type antibiotic. These kinds of antibiotics are widely used because they are inexpensive and easily accessible [3]. As a consequence of excessive consumption of 6-APA, it is frequently detected in the aquatic environment. This is an important problem due to its potential toxicity for human health and all living organisms [4]. Degradation reactions are very important for their removal from water. Their degradation products may lead to harmful results. The theoretical study of the oxidation mechanism of Dibutyl phthalate in gas and aqueous phase by hydroxyl and sulfate radicals can be given as an example to such reactions [5]. In some cases, the decomposition products can also be toxic or more toxic than the parent drug [6].

Therefore, antibiotics in water sources, especially drinking water sources, must be adequately treated due to their adverse effects on the ecosystem and human health. Special methods can be applied to remove pharmaceutical wastes, such as antibiotics, from water treatment plants. Advanced oxidation processes (AOPs) have been frequently used in recent years to remove environmental pollutants from water sources. The main mechanism of AOPs is the generation of highly reactive free radicals. The most reactive of the radicals formed are OH radicals. In the AOP technique, pollutants are decomposed through reactions with hydroxyl radicals [5, 7–10]. Thus, wastes such as antibiotics and micropollutants in the water are removed by OH radicals. There are some studies on antibiotic degradation with the AOP technique in the literature, but unfortunately, these are mostly for increasing the degradation rates [6, 11–17]. However, it is sometimes insufficient to fully explain the mechanism. Experimental methods involve long processes, are expensive, and also require equipment. Due to these difficulties in the experimental investigation of such reactions, quantum chemical computation methods are an important advantage [18, 19].

Quantum chemical computation methods are very useful for explaining the kinetic mechanism of reactions. In recent years, density functional theory (DFT) has been

✉ Arzu Hatipoglu
hatiparzu@yahoo.com

[1] Department of Chemistry, Yildiz Technical University, 34220 Istanbul, Turkey

used especially to investigate the kinetics of reactions at the molecular level due to its reliability and low cost [18]. The mechanisms, thermochemical properties, kinetic parameters of the reactions, and each possible reaction path can be determined by quantum chemical modeling methods [20]. In the literature, there are some studies about the degradation kinetics of antibiotics [21–24], but as far as we know, there is no quantum chemical computational kinetic study of the degradation reaction of 6-APA with the OH radical.

This study aims to examine in detail the kinetic mechanism of the degradation reaction of 6-APA with the OH radical. For this purpose, the rate constants and branching ratios of the reaction of 6-APA with the OH radical were calculated quantum chemically. Calculations were performed using different functionals of the DFT method. All kinetic and thermodynamic parameters were calculated in aqueous media using the conductor-like polarizable continuum model (CPCM) solvent model. Besides, the degradation reaction kinetics for the most probable reaction path were also investigated using explicit solvent models. The subsequent reaction mechanism for the most probable degradation product was proposed using Fukui functions.

Computational details

All calculations were performed using the DFT method in the Gaussian16 package program [25]. Different DFT functions such as B3LYP, M06-2X, and MPW1PW91 were used to find reliable kinetic results for the degradation kinetics of 6-APA. These functionals were developed to study organic reactions with a computational demand similar to the HF method [26]. It has been shown in some previous studies that B3LYP and MPW1PW91 functionals gave reliable results for oxidation reactions of organic compounds [4, 27]. Also, the M06-2X function was found suitable for kinetic and thermodynamic calculations and was proposed for such reactions [28]. In previous studies, B3LYP/6-31G(d,p) is the most suitable level of theory to predict the energy barriers of radical addition reactions [29, 30]. Based on these results, all the geometry optimizations were performed at 6-31G(d,p) level, followed by single point energy calculations at B3LYP/6–311 + G(d,p) level. Molecular electrostatic potential (MEP), frontier molecular orbital (FMO) analysis, and natural bond orbital (NBO) analysis were performed. All the molecular structure visualizations were prepared with the Gauss View 5.0 program [31].

All the reactants, pre-reactive complexes (PR), transition state complexes (TS), and products (P) were verified by frequency analyses. Transition state complexes were characterized by having one imaginary frequency. The ıntrinsic reaction coordinate (IRC) calculations were performed to understand the correlations of TS geometries with products and reactants along the reaction coordinate [32]. Zero-point vibrational energies (ZPEs) were calculated at the same level as the theory.

The thermodynamic parameters were calculated with standard statistical thermodynamic at 298.15 K and 1 atm. The reaction paths rate constants were calculated by using transition state theory with Wigner correction with the following equation:

$$k = K\frac{k_B T}{h} e^{\Delta G^{\ddagger}/RT} \tag{1}$$

$$\mathrm{K} = 1 + \frac{1}{24}\left[\frac{hI}{k_B T}\right]^2 \tag{2}$$

$$\delta = \frac{k_i}{k_{tot}} x100 \tag{3}$$

in which: κ is transmission coefficient, k_B is Boltzmann constant, h is Plank constant, T is the temperature, $\Delta G^{\#}$ is activation Gibbs free energy, I is the imaginar frequency of a transition state complex, k_{tot} is the total rate constant value, k_i is the rate constant value of each path, and δ is branching ratio [33, 34]. All the parameters were calculated manually.

Fukui functions are widely used for predicting reaction sites of the molecules. The larger the value of the Fukui functions, the higher the reactivity. There are three Fukui functions for nucleophilic attack f_i^+, electrophilic attack, f_i^-, and radical attack f_i^o. Fukui functions were calculated as defined in the equations below.

$$f_i^+ = q_i(N+1) - q_i(N) \tag{4}$$

$$f_i^- = q_i(N) - q_i(N-1) \tag{5}$$

$$f_i^o = \frac{f_i^+ - f_i^-}{2} \tag{6}$$

where $q_i\,(N)$, $q_i\,(N+1)$, and $q_i\,(N-1)$ are the electron densities of the i atom in the neutral, anionic, and cationic molecules, respectively [35, 36].

The aquatic effect on the reaction mechanism was investigated with explicit water molecules and an implicit solvent model (to describe bulk water behavior) CPCM with the dielectric constant value of water, $\varepsilon = 78.355$ [37]. It is known that in implicit solvent models, long-range interactions between solvent and solute are considered, but some important electronic interactions cannot be considered. The explicit solvent model with implicit solvents as the mixed model is a reasonable strategy for solvent–solute interactions [38]. Therefore, in this study, we have also explicitly investigated the increased 1 and 2 numbers of water molecules effect on the reaction kinetics. The addition of water molecules to the calculations was done one by one.

Results and discussion

Analysis of reaction paths

The degradation reaction of 6-APA with the hydroxyl radical can take place in two ways: (i) hydrogen abstraction of OH radicals from saturated bonds and (ii) OH radical addition to unsaturated bonds [28]. The calculated MEP, FMO, and NBO results are given in the Supplementary Materials. Concerning the MEP, FMO, and NBO results, the possible reaction paths of 6-APA with the OH radical are determined. These reaction paths include four possible hydrogen abstractions and two hydroxyl radical additions. As understood from the NBO results, the abstraction of hydrogens from the beta-lactam ring (the hydrogen atoms of C1 and C2) is sterically difficult because these atoms are not as electrophlic as the other hydrogen atoms. All possible initial degradation paths are shown in Fig. 1 and Scheme 1. Paths 1, 2, 3, and 4 are the hydrogen abstraction paths, and paths 5 and 6 are the hydroxyl radical addition paths.

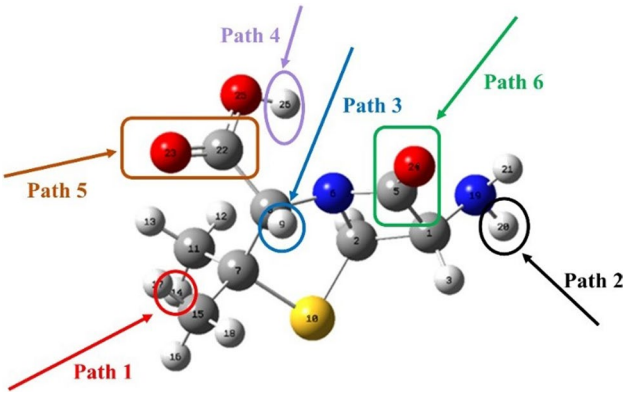

Fig. 1 Possible reaction paths for 6-APA

Degradation reaction mechanism

Abstraction paths

Optimized geometries of pre-reactive complexes, transition state complexes, and products for hydrogen abstraction reaction paths are given in Fig. 2 for B3LYP/6-31G(d,p). The potential energy graph for these reaction paths is given in Fig. 3. Optimized geometries of structures and potential energy graphs for other functionals are also given in the Supplementary Material.

The pre-reactive complexes are important for the reaction paths because they lower the activation energies.

Scheme 1. Initial degradation paths for 6-APA

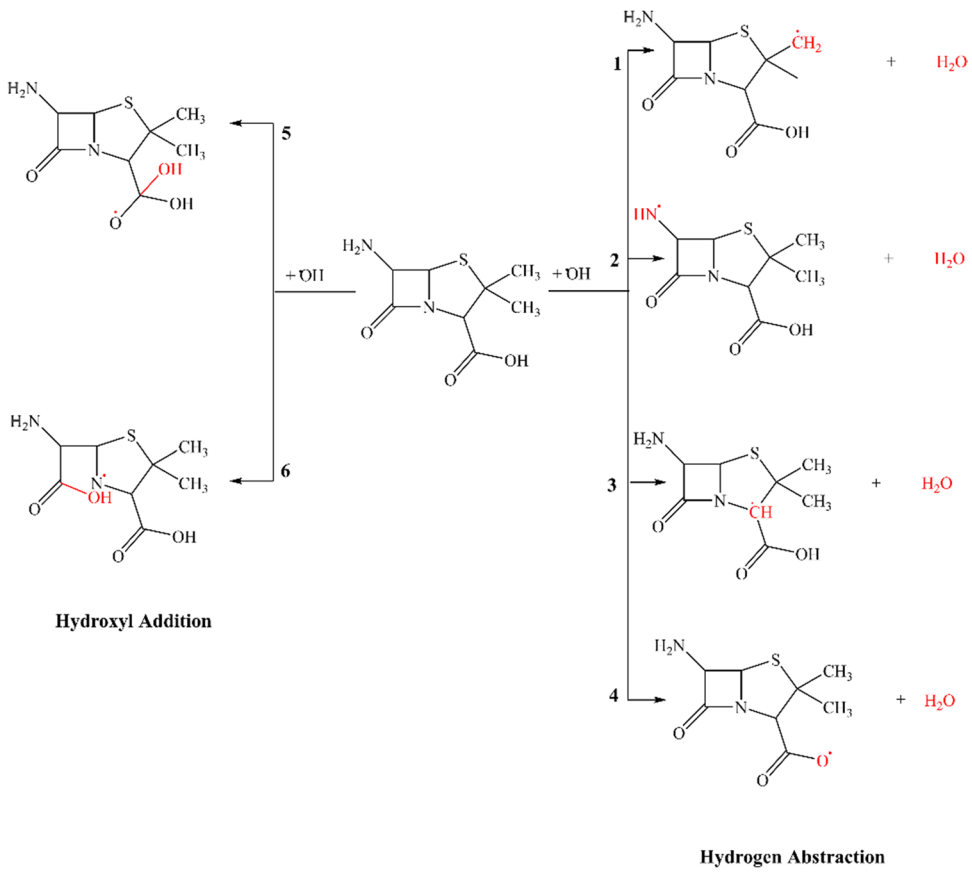

These complexes have lower energies than reactants due to hydrogen bonds or Van der Waals attraction [39]. According to the preliminary calculation results, four different pre-reactive complexes are formed in the 6-APA reaction with OH radicals, as shown in Scheme 1. The major changes in the geometries of the optimized pre-reactive complexes are observed in the bonds between the oxygen atom of OH and the C or N atom, to which the hydrogen atom is to be abstracted in 6-APA. In the PR1 complex, there is a 2.29 Å Van der Waals interaction between the oxygen atom of the OH radical and the hydrogen of C11, and the angle between the hydroxyl radical and C11 is 98.52°. In PR2, a hydrogen bond of 1.67 Å length is formed between the oxygen atom of the OH radical and the hydrogen atom of N19. The angle between the OH radical and the N19 atom is 106.34° in PR2. As seen in Fig. 2, there are two interactions in the PR3 complex. They are 1.92 Å and 2.37 Å long bond lengths between the OH radical and the O24 and hydrogen of C8 atoms, respectively. The angle between the OH radical and the C8 atom in PR3 is 80.36°. In the PR4 complex, there are also two hydrogen bond interactions with the OH radical. They have 1.93 Å and 1.82 Å bond lengths with the hydrogen of O23 and the N19 atom, respectively. The angle between the OH radical and hydrogen atom of O23 is 112.62°. As seen in Fig. 3, PR4 has the lowest energy. This may be the result of the two hydrogen bond interactions in PR4, and these bond lengths are shorter than the others. As seen in the potential energy graph, the energies of the pre-reactive complexes are 0.63, 5.02, 4.39, and 12.99 kcal·mol^{-1} lower than those of the reactants, respectively. The energetically most stable complex is PR4.

For each of the possible reaction paths, four transition state complexes are identified. In the formation of transition state complexes, the main geometric changes are observed around the atom from which the hydrogen is abstracted. While the C-X or N-X bonds to which the hydrogen is abstracted are lengthening, the lengths of the subsequent

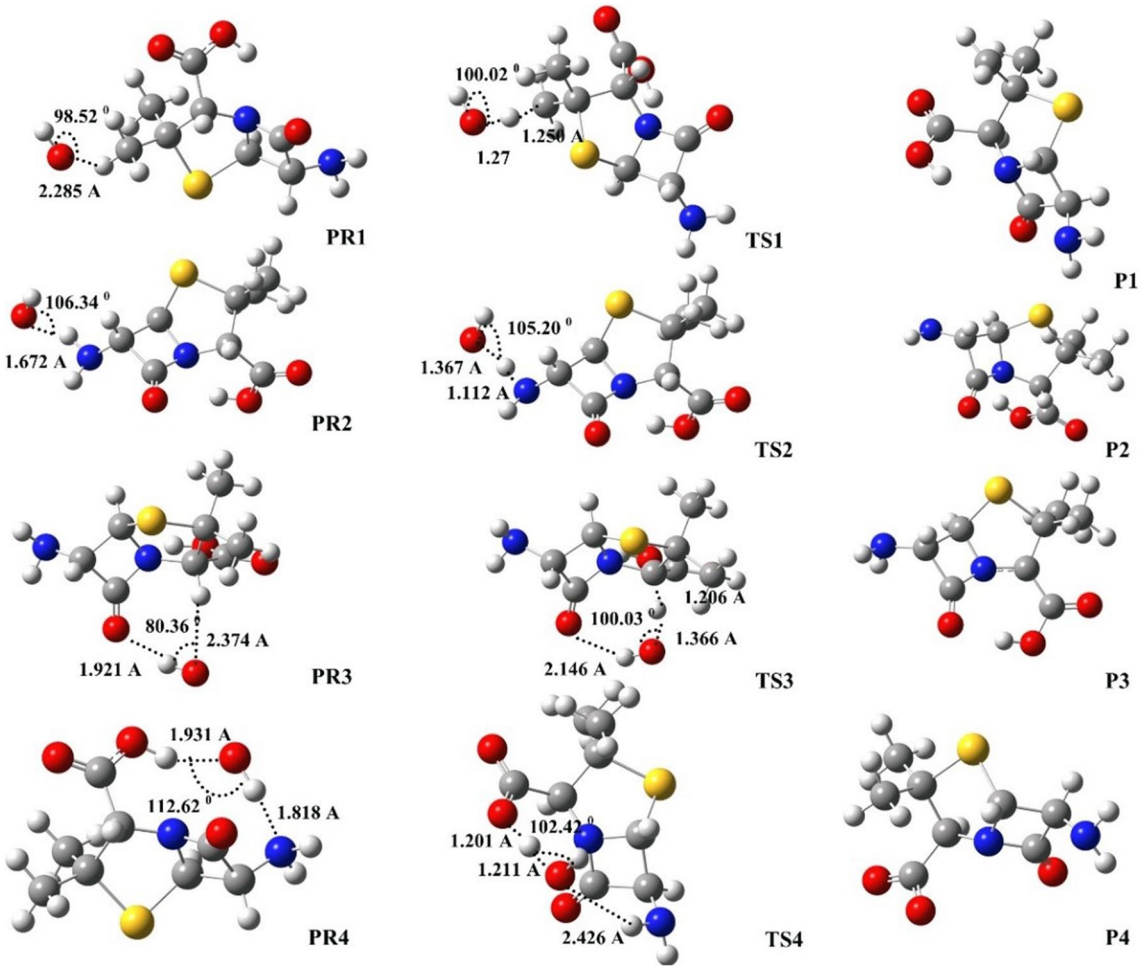

Fig. 2 Optimized geometries of pre-reactive complexes, transition state complexes, and products for hydrogen abstraction reaction paths for B3LYP/6-31G(d,p)

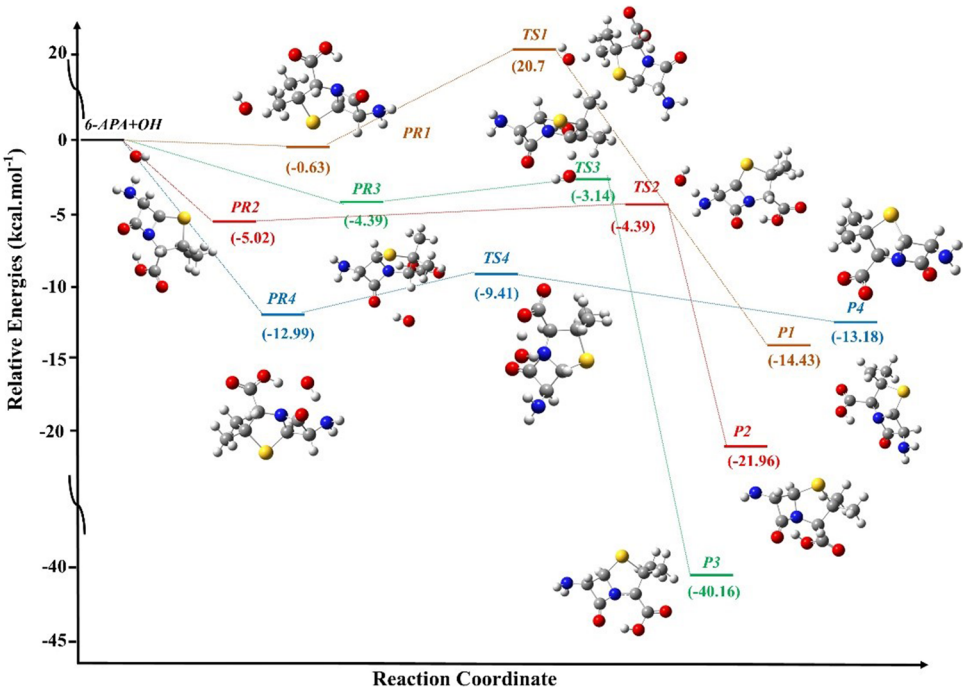

Fig. 3 Potential energy diagram for hydrogen abstraction paths for B3LYP/6-31G(d,p)

bonds remain the same. In the transition state complexes, the breaking bond lengths C-H and N–H of 6-APA are 1.25 Å, 1.11 Å, 1.21 Å, and 1.20 Å. The elongation in broken bonds is 0.16, 0.09, 0.11, and 0.22 Å for TS1, TS2, TS3, and TS4, respectively. The length of the O–H bond formed is also important in the formation of TS complexes along the reaction coordinate. The occurring O–H bond lengths are 1.27 Å, 1.37 Å, 1.37 Å, and 1.21 Å for TS1, TS2, TS3, and TS4, respectively. So these structures are early transition states that resemble reactants, as stated in Hammond's postulate [40]. In transition state structures, the angles between the approaching OH radical and the abstracted hydrogen atoms average 101.92°. As seen in the potential energy diagram (Fig. 3), all transition state complexes have higher energy than pre-reactive complexes. The TS energies except TS1 are below the energies of the reactants, and we can order their stability TS4 > TS2 > TS3 > TS1. The energies of the transition state complexes are 21.34, 0.63, 1.25, and 3.58 kcal/mol higher than those of the pre-reactive complexes, respectively.

Addition paths

The optimized geometries of the pre-reactive complexes, transition state complexes, and products formed in hydroxyl radical addition paths and the potential energy graphs are given in the Supplementary Material.

In the pre-reactive complexes PR5 and PR6, the C-O bond lengths of the OH radical and the C5 and C22 atoms are 3.40 Å and 3.50 Å, respectively. In the pre-reactive complex structures, the bond angle with the OH radical is approx. 91.61°. For TS structures, the length of the C-O bonds formed by the interaction of the hydroxyl radical and carbonyl groups is 1.88 (C5) Å and 1.99 (C22) Å for TS5 and TS6, respectively. The angle between carbonyl groups and the OH radical in TS5 and TS6 is approximately 101.92°. As seen in the potential energy diagram in the supplementary file, the energy of TS5 is higher than that of the reactants and TS6.

In this study, functional effects on molecular geometry are also tried to understand. The obtained transition state complex structures for path 6 are given together for different functionals. Interestingly, it is seen that functional differences have no important effect on the molecular geometries of the transition state complex structures. It is understood from Fig. 4 that no matter what functionals are used, similar structures are found. In Domingo's study [26], the same results were also found for the structure of transition state complexes.

Energetic and kinetic parameters

The calculated thermodynamic parameters for hydrogen abstraction and OH-addition reaction paths are given in Table 1. As can be seen from Table 1, the Gibbs free energy of path 5 is positive for all three functionals. Therefore, it can be concluded that path 5 is a thermodynamically nonspontaneous process. The most negative enthalpy and Gibbs free energies belong to path 6, with values of − 47.24 kcal/mol and − 38.57 kcal/mol (B3LYP). So, with the addition of OH radical to the carbonyl group of the beta-lactam unit,

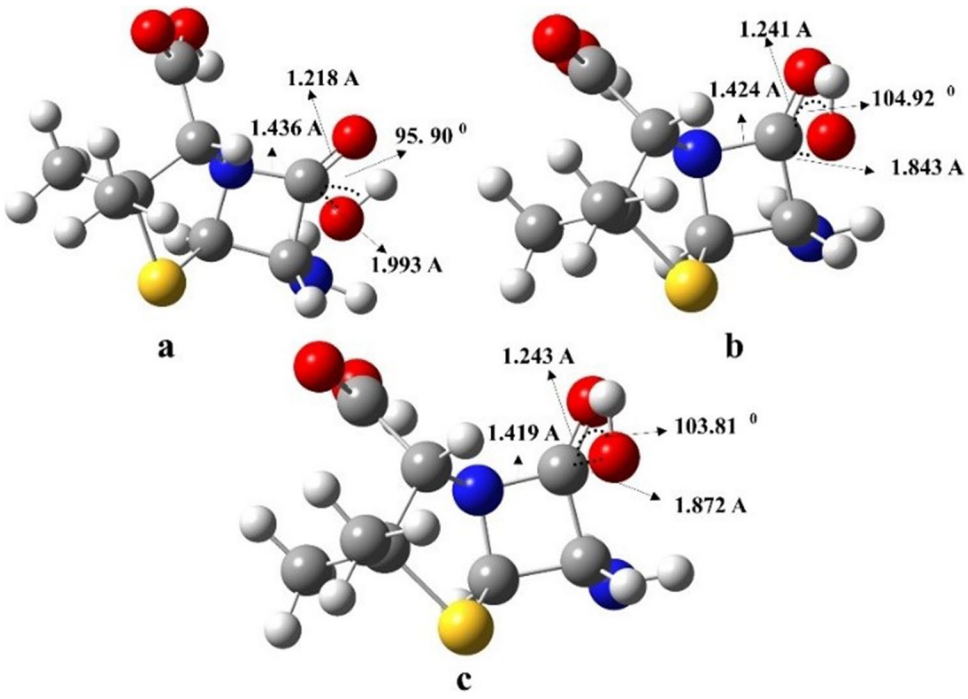

Fig. 4 Optimized geometries of transition state complexes' structures for path 6 **a** B3LYP, **b** M06-2X, **c** MPW1PW91

path 6 spontaneously occurs with its exergonic nature. This result is also compatible with some experimental degradation studies [41–43]. The order in the calculated Gibbs free energies is path 6 < path 3 < path2 < path1 < path 4 < path 5. This order is the same for the reactions enthalpies. All DFT functionals used have the same energy order as seen in Table 1.

The calculated kinetic parameters of the 6-APA with the OH radical are listed in Table 2. As seen in Table 2, the lowest activation Gibbs free energy belongs to path 6, and the highest one belongs to path 1. This result is also the same for rate constants and branching ratios. Among the reaction paths, the OH-addition reaction from the beta-lactam ring of 6-APA, path 6, is the one that will most likely occur. Among the hydrogen abstraction paths, the smallest activation Gibbs free energy belongs to path 4, hydrogen abstraction from the carboxylic acid end. This path is the second possible reaction path, as seen from its branching ratio. Among the all hydrogen abstraction paths for hydrogen abstraction from the methyl group, path 1 has a minor effect on the reaction kinetics. The total rate constant value calculated according to B3LYP is closer to the experimentally obtained value than the total rate constant results of other functionals [44]. We can conclude that B3LYP gives better results for the 6-APA degradation reaction. Similar results were found in the Rajakumar et al. study for the OH radical degradation reaction with bromine oxide [45].

In order to show the effectiveness of a higher base set on the results, a single point energy calculation was done with the B3LYP/6–311 + G(d,p) basis set [30]. All the results are given in the Supplementary Materials. As seen in Table S3, the rate constant is more consistent with the experimental value when calculating with a higher basis set.

Table 1 Enthalpies (ΔH, kcal/mol) and Gibbs free energies (ΔG, kcal/mol) for different functionals

	B3LYP		M06-2X		MPW1PW91	
	ΔH	ΔG	ΔH	ΔG	ΔH	ΔG
1	− 12.89	− 14.79	− 14.95	− 16.71	− 10.68	− 11.96
2	− 19.40	− 20.33	− 17.20	− 18.40	− 14.02	− 15.05
3	− 36.25	− 37.51	− 32.47	− 34.13	− 30.61	− 32.36
4	− 10.58	− 13.21	− 2.79	− 4.59	− 3.37	− 5.23
5	− 5.09	5.71	− 8.63	2.42	− 6.62	4.48
6	− 47.24	− 38.57	− 48.50	− 40.73	− 46.08	− 36.66

Table 2 Calculated kinetic parameters, I (cm^{-1}), $\Delta G^{\#}$ (kcal/mol), k (M^{-1} s^{-1})

	B3LYP				M06-2X				MPW1PW91			
	I	$\Delta G^{\#}$	k_{calc}	δ	I	$\Delta G^{\#}$	k_{calc}	δ	I	$\Delta G^{\#}$	k_{calc}	δ
1	−1338.24	8.22	5.82×10^{6}	2.55×10^{-3}	−1583.48	4.65	2.42×10^{9}	0.10	−1448.66	9.03	1.49×10^{6}	3.96×10^{-4}
2	−791.29	3.92	8.27×10^{9}	3.63	−814.08	1.69	3.60×10^{11}	15.45	−959.46	5.68	4.28×10^{8}	0.11
3	−837.03	3.64	1.33×10^{10}	5.83	−1518.74	2.86	4.98×10^{10}	2.13	−946.18	3.67	1.27×10^{10}	3.37
4	−1281.93	2.96	4.15×10^{10}	18.20	−353.46	2.74	6.09×10^{10}	2.61	−685.20	2.46	9.76×10^{10}	25.96
5	−432.25	5.25	8.80×10^{8}	0.39	−612.15	3.41	1.96×10^{10}	0.84	−1363.31	3.67	1.28×10^{10}	3.40
6	−641.10	2.15	1.64×10^{11}	71.93	−203.93	0.72	1.84×10^{12}	78.86	−493.26	1.90	2.53×10^{11}	67.29
k_{tot}			2.28×10^{11}				2.33×10^{12}				3.76×10^{11}	
$\log k_{tot}$			11.36				12.37				11.58	
$\log k_{exp}$ [44]			9.38				9.38				9.38	

Effect of explicit water molecules on the reaction kinetic

Adding some discrete water molecules to the implicit computation is an important strategy to explain the effect of water on the reaction. This is less costly and simpler for getting good, comparable results with experimental ones [46].

The effects of discrete solvent water molecules on the reaction kinetics are also investigated. Because of the high computational time demands of this type of calculation, explicit solvent model calculations are only performed for the most probable reaction path, path 6. Thus, 1 and 2 open water molecules are added to the reaction coordinate to test the water environment effect (0 water model is the pure implicit model). For the selected reaction path, the addition of water for the pre-reactive and transition state complexes, and products is done one at a time in the reaction center. After the addition of water molecules to each structure, re-optimizations are performed by allowing all added water molecules to interact with the 6-APA molecule. The optimized structures by adding the explicit water molecules for path 6 are given in Fig. 5. IRC calculations were performed to confirm the transition state that connected the true reactants and products for path 6, and these plots are given in Fig. 6. The potential energy diagrams for the explicit solvent models are given in the Supplementary Material.

In one water model, the stabilization of the pre-reactive complex occurs by forming hydrogen bonding between the oxygen of the water molecule and the hydrogen atom of O25 with a distance of 1.71 Å. In this pre-reactive structure, the approaching distance of the OH radical to C5 is 3.01 Å which is 0.01 Å smaller than the same bond in the 0 water model. In the transition state complex structure, the distance between the OH radical and the C5 atom is 2.09 Å. In this complex, two hydrogen bonds occurred by hydrogen of O25 and oxygen of water is 1.71 A and hydrogen of water and O24 is 1.87 Å. The obtained product structure in 1 water model contains two different extra hydrogen bondings with oxygen of water and hydrogen of O23 and oxygen of water and hydrogen of C8 bond lengths of 1.93 Å and 2.42 Å, respectively. It is seen from Fig. 5 the pre-reactive complex of 2 waters model, explicitly added water molecules interacts with O25, oxygen of hydroxyl radical, and hydrogen of C8 atom with bond lengths of 2.19 Å, 2.18 Å, and 1.71 Å, respectively. In the transition state complex structure for the 2 waters model, the bond distance between the oxygen atom of OH radical and the C5 atom of the 6-APA molecule is 1.74 Å. The transition state structure is stabilized by hydrogen bondings between hydrogen atoms of water molecules and 6-APAs' of O24 atom with distances of 1.90 Å and 1.79 Å, respectively. In product structure, three hydrogen bonds occurred with water molecules, hydrogen of C8 and O24, and hydrogen of N19, with bond lengths of 2.44 Å, 1.93 Å, and 2.00 Å, respectively.

Hydrogen bonds are important attractions for occurring pre-reactive complexes, transition state complexes, and products. As a result of these attractions, the energy of the molecules decreased and their stabilization increased. As seen in Fig. 5, for the 1 water model, the addition of water molecules results in molecular attraction, and the hydroxyl radical distance to the C5 atom is 0.098 Å higher than for the 0 water model. This distance is 0.251 Å smaller than the transition state complex found for the 2 waters model. In the explicit 2 waters model, the OH radical can approach the carbonyl group in the beta-lactam ring more easily than in the implicit model. That, in turn, affects the reaction properties.

The calculated thermodynamic and kinetic parameters for 0 water, 1 water, and 2 water models are given in Table 3. It is seen from Table 3, one and two water models are the exergonic paths, and their enthalpy and Gibbs free energy values are all negative. The activation Gibbs free energy value in the pure implicit model is 2.15 kcal/mol. As the number of explicit water molecules increases, the Gibbs free energy also increases. Accordingly, as can be seen from Table 3, the reaction rate also decreases. In the reaction mechanism, hydrogen bonds formed between 6-APA and the oxygen atom of the water molecule cause the

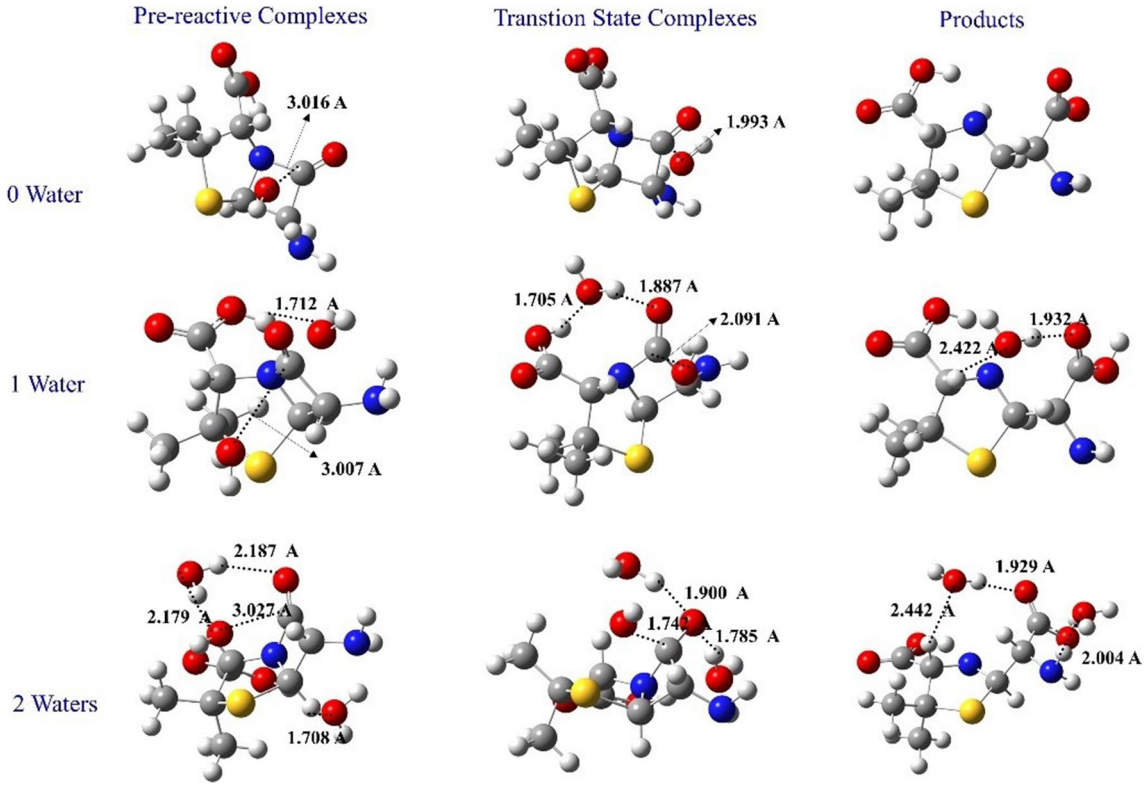

Fig. 5 Optimized geometries of pre-reactive complexes, transition state complexes, and products for varying number of water molecules

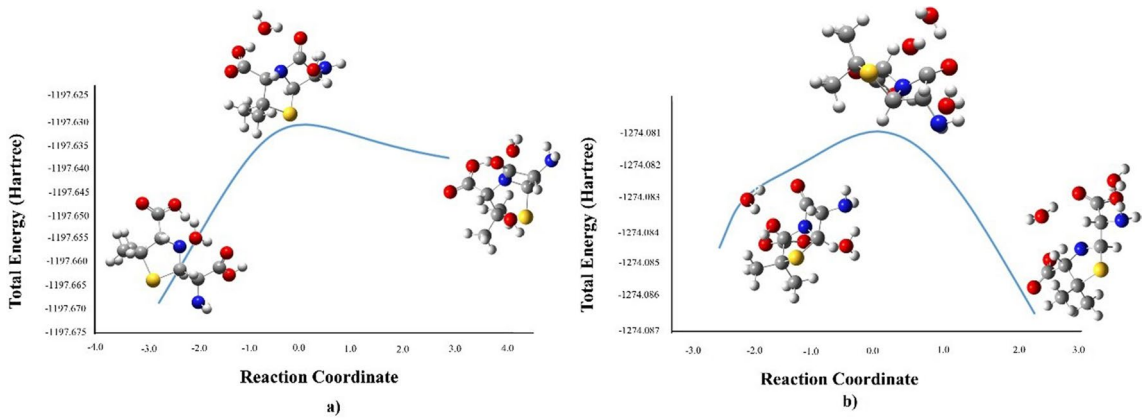

Fig. 6 IRC plots for path 6 **a** 1 water model and **b** 2 waters model

reaction to be suppressed. Thus, as the number of explicitly added water molecules increases, the relative energies of the structures increase, and the molecular system becomes unstable. Because, during the investigation of the reaction with explicit water molecules, the water molecules can form hydrogen bonds with each other and with 6-APA. Adding more water molecules makes the theoretical degradation kinetic model results more compatible with the experimental ones. The addition of explicit water molecules causes the relative energies of the structures to increase, as seen in Table 3. Thus, instability occurs in the molecular system, and thus the Gibbs activation free energy increases. In addition, as can be seen from the entropy values, as the number of water molecules increases, the entropy increases due to the disorder. As a result, instability occurs in the molecular system, resulting in an increase in Gibbs activation free energy. Therefore, it can be concluded that 2 waters model can be used for the degradation kinetics of other penicillin derivatives. Ideally, working with explicit water molecules yields results closer to the experimental results, although

Table 3 Calculated thermodynamic and kinetic parameters for path 6

	Explicit models		
	0 Water	1 Water	2 Waters
ΔH (kcal/mol)	−47.24	−37.41	−37.41
ΔS (cal/mol/K)	−29.08	0.67	2.08
ΔG (kcal/mol)	−38.57	−37.61	−38.03
I (cm^{-1})	−641.10	−479.79	−258.26
$\Delta G^{\#}$ (kcal/mol)	2.15	2.94	5.95
k_{calc} (M^{-1} s^{-1})	1.64×10^{11}	4.31×10^{10}	2.67×10^{8}
$\log k_{calc}$ (M^{-1} s^{-1})	11.21	10.63	8.43

the computational difficulties and numerous configurations make it very unwieldy. Therefore, it can be concluded that 2 waters model can be used for the degradation kinetics of other beta-lactam derivative antibiotics.

Subsequent processes of the P6

The Fukui functions of atoms in P6 were calculated to examine the plausible subsequent processes of the most probable product, P6. The optimized geometric structure and Fukui functions of P6 are given in Fig. 7, and the predicted degradation mechanism is given in Scheme 2.

The atoms with a larger Fukui functions value are the possible reaction sites. As demonstrated in Fig. 7b, N6 and S10 are suitable sites for electrophilic hydroxyl radical attack. In path A, hydroxyl radical attack to S10 atom in the thiazolidine ring leads to the production of an oxidation product. Then PA is obtained by hydrogen abstraction of the hydroxyl radical from the carbon atom near the nitrogen atom (N6) of the oxidation product. Serna-Galvis et al. obtained a similar product in the degradation study of oxacillin, a beta-lactam type antibiotic [47]. In path B and path C,

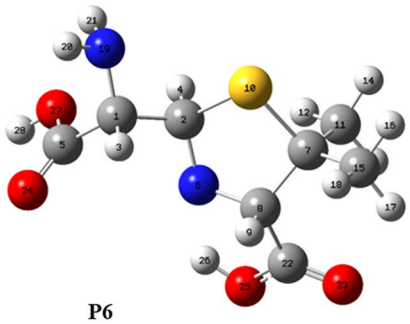

a

P6	q(N)	q(N+1)	q(N-1)	f_i^+	f_i^-	f_i^o
C1	6.006	5.984	6.036	-0.022	-0.030	-0.026
C2	6.087	6.008	6.147	-0.080	-0.059	-0.070
C5	5.410	5.422	5.377	0.012	0.032	0.022
N6	7.383	7.728	7.275	0.345	0.109	0.227
C7	6.130	6.097	6.172	-0.033	-0.042	-0.037
C8	6.018	5.941	6.045	-0.078	-0.026	-0.052
S10	15.935	16.083	15.664	0.149	0.271	0.210
C11	6.311	6.302	6.324	-0.009	-0.013	-0.011
C15	6.318	6.314	6.322	-0.004	-0.004	-0.004
N19	7.606	7.623	7.541	0.017	0.065	0.041
C22	5.383	5.425	5.344	0.042	0.039	0.040
O23	8.486	8.528	8.429	0.041	0.057	0.049
O24	8.490	8.513	8.443	0.023	0.047	0.035
O25	8.498	8.522	8.470	0.024	0.028	0.026
O27	8.492	8.498	8.480	0.006	0.012	0.009

b

Fig. 7 **a** Optimized geometry for P6 and **b** Mulliken charge populations and Fukui functions of P6

Scheme 2. Possible subsequent reaction mechanism of P6

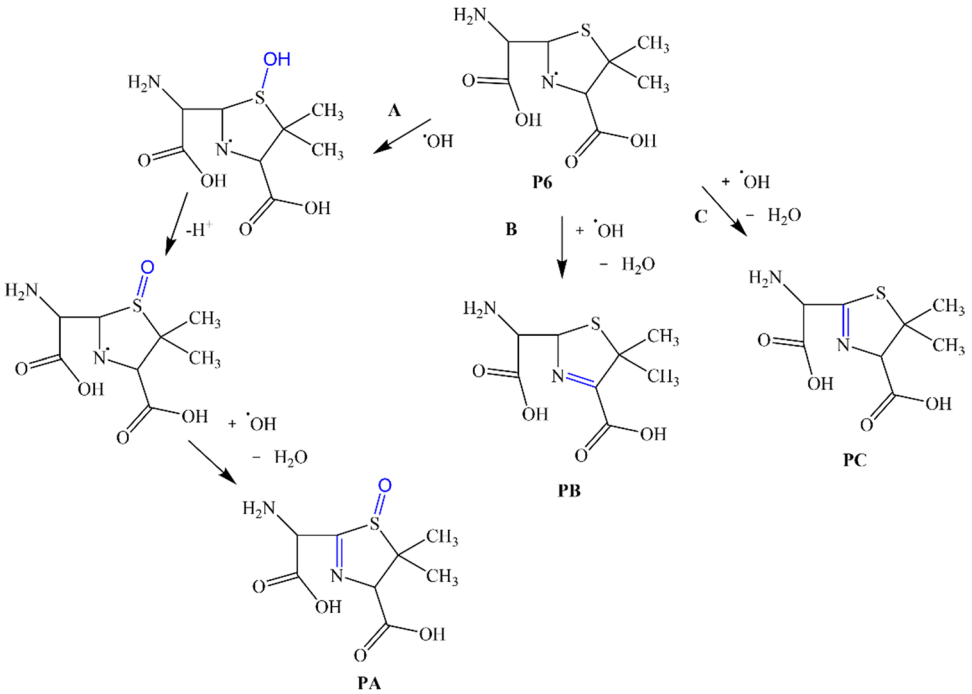

products of hydrogen atoms abstracted from C atoms bound to reactive N6 are proposed. In these paths, PB and PC are formed as a result of hydrogen abstraction from the unsaturated thiazolidine ring. Similar reactions and products were obtained in experimental studies [22, 47–49].

Conclusions

In this study, the degradation kinetics of 6-APA with hydroxyl radicals are investigated by the DFT method with different functionals. The comparison between the three functions shows that the B3LYP results are more consistent with the experimental results than the M06-2X and MPW1PW91. The calculated kinetic and thermodynamic parameters, reaction enthalpies, and Gibbs free energies demonstrate that the OH-addition path is more favorable than the H-abstraction path. It was found that OH radical addition to the carbonyl group of the beta-lactam ring (path 6) is the most favorable path. Water molecules affect the degradation reaction mechanism. As the number of solvent water increases, the results of the explicit model are in agreement with those obtained experimentally. The energy of the molecular system increases with the addition of explicit water molecules, and accordingly, the reaction rate constant decreases. With the addition of two water molecules, the rate constant is more in agreement with the experimental results. It can be concluded that the results of the explicit water model play an important role in estimating the experimental degradation kinetic rate constant. Finally, possible subsequent reactions of P6 were also examined. The proposed end products are compatible with the literature. Therefore, such theoretical studies will be informative in terms of understanding the degradation kinetics of other beta-lactam-derived antibiotics.

Supplementary Information The online version contains supplementary material available at https://doi.org/10.1007/s00894-023-05636-y.

Author contribution AH: conceptualization, writing—reviewing and editing. SA: DFT calculations, writing.

Funding This study is supported by Yildiz Technical University Research Coordination with Project number FDK-2021–4138. We also acknowledge computational resources that are provided by TÜBİTAK ULAKBİM, High Performance and Grid Computing Center (TRUBA).

Data availability It will be given if it is necessary.

Code availability It will be given if it is necessary.

Declarations

Conflict of interest The authors declare no competing interests.

References

1. Ioannou-Ttofa L, Raj S, Prakash H, Fatta-Kassinos D (2019) Solar photo-Fenton oxidation for the removal of ampicillin, total cultivable and resistant E. coli and ecotoxicity from secondary-treated wastewater effluents. Chem Eng J 355:91–102. https://doi.org/10.1016/j.cej.2018.08.057
2. Charuaud L, Jarde E, Jaffrezic A, Thomas MF, Le Bot B (2019) Veterinary pharmaceutical residues from natural water to tap water: sales, occurrence and fate. J Hazard Mater 361:169–186
3. Deshpande AD, Baheti KG, Chatterjee NR (2004) Current science association degradation of β-lactam antibiotics.Curr Sci 87:1684–1695. https://www.jstor.org/stable/24109765
4. Xiao R, Noerpel M, Ling Luk H, Wei Z, Spinney R (2014) Thermodynamic and kinetic study of ibuprofen with hydroxyl radical: a density functional theory approach. Int J Quantum Chem 114:74–83. https://doi.org/10.1002/qua.24518
5. Li H, Zhang Y, Wan J, Xiao H, Chen X (2018) Theoretical investigation on the oxidation mechanism of dibutyl phthalate by hydroxyl and sulfate radicals in the gas and aqueous phase. Chem Eng J 339:381–392. https://doi.org/10.1016/j.cej.2017.12.153
6. Szabó L, Tóth T, Rácz G, Takács E, Wojnárovits L (2016) •OH and e-aq are yet good candidates for demolishing the β-lactam system of a penicillin eliminating the antimicrobial activity. Radiat Phys Chem 124:84–90. https://doi.org/10.1016/j.radphyschem.2015.10.012
7. Arslan-Alaton I, Dogruel S (2004) Pre-treatment of penicillin formulation effluent by advanced oxidation processes. J Hazard Mater 112:105–113. https://doi.org/10.1016/j.jhazmat.2004.04.009
8. Michael I, Rizzo L, McArdell CS, Manaia CM, Merlin C, Schwartz T, Dagot C, Fatta-Kassinos D (2013) Urban wastewater treatment plants as hotspots for the release of antibiotics in the environment: a review. Water Res 47:957–995
9. Wols BA, Hofman-Caris CHM (2012) Review of photochemical reaction constants of organic micropollutants required for UV advanced oxidation processes in water. Water Res 46:2815–2827
10. He X, Mezyk SP, Michael I, Fatta-Kassinos D, Dionysiou DD (2014) Degradation kinetics and mechanism of β-lactam antibiotics by the activation of H2O2 and Na2S2O8 under UV-254nm irradiation. J Hazard Mater 279:375–383. https://doi.org/10.1016/j.jhazmat.2014.07.008
11. Serna-Galvis EA, Silva-Agredo J, Giraldo AL, Flórez-Acosta OA, Torres-Palma RA (2016) Comparative study of the effect of pharmaceutical additives on the elimination of antibiotic activity during the treatment of oxacillin in water by the photo-Fenton, TiO2-photocatalysis and electrochemical processes. Sci Total Environ 541:1431–1438. https://doi.org/10.1016/j.scitotenv.2015.10.029
12. Yabalak E, Döndaş HA, Gizir AM (2017) Subcritical water oxidation of 6-aminopenicillanic acid and cloxacillin using H2O2, K2S2O8, and O2. J Environ Sci Health A Tox Hazard Subst Environ Eng 52:210–220. https://doi.org/10.1080/10934529.2016.1246935
13. Bansal P, Verma A (2017) Synergistic effect of dual process (photocatalysis and photo-Fenton) for the degradation of Cephalexin using TiO2 immobilized novel clay beads with waste fly ash/foundry sand. J Photochem Photobiol A Chem 342:131–142. https://doi.org/10.1016/j.jphotochem.2017.04.010
14. Yabalak E (2018) An approach to apply eco-friendly subcritical water oxidation method in the mineralization of the antibiotic ampicillin. J Environ Chem Eng 6:7132–7137. https://doi.org/10.1016/j.jece.2018.10.010
15. Al-Musawi TJ, Kamani H, Bazrafshan E, Panahi AH, Silva MF, Abi G (2019) Optimization the effects of physicochemical parameters on the degradation of cephalexin in sono-Fenton reactor by

using Box-Behnken response surface methodology. Catal Letters 149:1186–1196. https://doi.org/10.1007/s10562-019-02713-x
16. Mirzaei A, Haghighat F, Chen Z, Yerushalmi L (2019) Sonocatalytic removal of ampicillin by Zn(OH)F: effect of operating parameters, toxicological evaluation and by-products identification. J Hazard Mater 375:86–95. https://doi.org/10.1016/j.jhazmat.2019.04.069
17. Baran W, Adamek E, Jajko M, Sobczak A (2018) Removal of veterinary antibiotics from wastewater by electrocoagulation. Chemosphere 194:381–389. https://doi.org/10.1016/j.chemosphere.2017.11.165
18. Li H, Miao X, Zhang J, Du J, Xu S, Tang J, Zhang Y (2020) DFT studies on the reaction mechanism and kinetics of dibutyl phthalate initiated by hydroxyl and sulfate radicals: prediction of the most reactive sites. Chemical Engineering Journal 381. https://doi.org/10.1016/j.cej.2019.122680
19. Sanches-Neto FO, Ramos B, Lastre-Acosta AM, Teixeira ACSC, Carvalho-Silva VH (2021) Aqueous picloram degradation by hydroxyl radicals: unveiling mechanism, kinetics, and ecotoxicity through experimental and theoretical approaches. Chemosphere 278. https://doi.org/10.1016/j.chemosphere.2021.130401
20. Mishra BK, Chakrabartty AK, Deka RC (2013) Theoretical study on rate constants for the reactions of CF 3CH2NH2 (TFEA) with the hydroxyl radical at 298 K and atmospheric pressure. J Mol Model 19:2189–2195. https://doi.org/10.1007/s00894-013-1762-7
21. Xu L, Li W, Désesquelles P, Van-Oanh NT, Thomas S, Yang J (2019) A statistical model and DFT study of the fragmentation mechanisms of metronidazole by advanced oxidation processes. J Phys Chem A 123:933–942. https://doi.org/10.1021/acs.jpca.8b10554
22. Belhacova L, Bibova H, Marikova T, Kuchar M, Zouzelka R, Rathousky J (2021) Removal of ampicillin by heterogeneous photocatalysis: combined experimental and dft study. Nanomaterials 11. https://doi.org/10.3390/nano11081992
23. Zeng X, Meng Y, Shu S, Guo F (2022) Density functional theory investigation on aqueous degradation mechanism of norfloxacin initiated by hydroxyl radical. Struct Chem 33:1213–1222. https://doi.org/10.1007/s11224-022-01928-w
24. Aydogdu S, Hatipoglu A (2023) Theoretical insights into the reaction mechanism and kinetics of ampicillin degradation with hydroxyl radical. J Mol Model 29:63. https://doi.org/10.1007/s00894-023-05462-2
25. Frisch MJ, Trucks GW, Schlegel HB, Scuseria GE, Robb MA,Cheeseman JR, Scalmani G, Barone V, Petersson GA, NakatsujiH, Li X, Caricato M, Marenich AV, Bloino J, Janesko BG,Gomperts R, Mennucci B, Hratchian HP, Ortiz JV, Izmaylov AF,Sonnenberg JL, Williams-Young D, Ding F, Lipparini F, EgidiF, Goings J, Peng B, Petrone A, Henderson T, Ranasinghe D,Zakrzewski VG, Gao J, Rega N, Zheng G, Liang W, Hada M,Ehara M, Toyota K, Fukuda R, Hasegawa J, Ishida M, NakajimaT, Honda Y, Kitao O, Nakai H, Vreven T, Throssell K, MontgomeryJA, Peralta Jr. JE, Ogliaro F, Bearpark MJ, Heyd JJ, BrothersEN, Kudin KN, Staroverov VN, Keith TA, Kobayashi R, NormandJ, Raghavachari K, Rendell AP, Burant JC, Iyengar SS, Tomasi J,Cossi M, Millam JM, Klene M, Adamo C, Cammi R, OchterskiJW, Martin RL, Morokuma K, Farkas O, Foresman JB, Fox DJ(2016) Gaussian 16, Revision C.01 Gaussian, Inc., Wallingford
26. Domingo LR (2016) Molecular electron density theory: a modern view of reactivity in organic chemistry. Molecules 21. https://doi.org/10.3390/molecules21101319
27. Gulvi NR, Patel P, Maliekal PJ, Badani PM (2021) Effect of substitution on dissociation kinetics of C2H5X, (X = F, Cl, Br and I): a theoretical study. Mol Phys 119. https://doi.org/10.1080/00268976.2020.1807635
28. Gour NK, Borthakur K, Paul S, Chandra Deka R (2020) Tropospheric degradation of 2-fluoropropene (CH3CF[dbnd]CH2) initiated by hydroxyl radical: reaction mechanisms, kinetics and atmospheric implications from DFT study. Chemosphere 238. https://doi.org/10.1016/j.chemosphere.2019.124556
29. Özen AS, Aviyente V, Klein RA (2003) Modeling the oxidative degradation of azo dyes: a density functional theory study. J Phys Chem A 107:4898–4907. https://doi.org/10.1021/jp026287z
30. Ruff F, Szabó D, Rábai J, Jalsovszky I, Farkas Ö (2019) Mechanism for the reactions of sulfides with hypochlorous acid and N-chlorosulfon-amides: formation of solvated chlorosulfonium cation and λ4-sulfane intermediates. J Phys Org Chem 32. https://doi.org/10.1002/poc.4005
31. Dennington R, Keith TA, Millam JM (2016) GaussView, Version5.0. Semichem Inc., Shawnee Mission, KS
32. Gonzalez C, Schlegel HB (1990) Reaction path following in mass-weightedinternal coordinates Cartesians and with internal coordinateswithout mass-weighting. J Phys Chem 94:5523. https://doi.org/10.1021/j100377a021
33. Saïd AE hadj, Mekelleche SM (2021) Antioxidant activity of Trolox derivatives toward methylperoxyl radicals: thermodynamic and kinetic theoretical study. Theor Chem Acc 140. https://doi.org/10.1007/s00214-021-02815-z
34. Levine IN (2009) Physical Chemistry, 6th edn. Mc Graw Hill-Higher Education, New York
35. Yang W, Parr RG (1985) Hardness, softness, and the Fukui function in the electronic theory of metals and catalysis. Proc Nati Acad Sci 82:6723–6726
36. Gurkan YY, Turkten N, Hatipoglu A, Cinar Z (2012) Photocatalytic degradation of cefazolin over N-doped TiO 2 under UV and sunlight irradiation: prediction of the reaction paths via conceptual DFT. Chem Eng J 184:113–124. https://doi.org/10.1016/j.cej.2012.01.011
37. Foresman J, Frish E (1996) Exploring chemistry. Gaussian Inc, Pittsburg
38. Khatri V, Dhattarwal HS, Kashyap HK, Singh G (2021) First-principles based theoretical investigation of impact of polyolefin structure on photooxidation behavior. J Comput Chem 42:1710–1719. https://doi.org/10.1002/jcc.26702
39. Hatipoglu A, Vione D, Yalçin Y, Minero C, Çinar Z (2010) Photooxidative degradation of toluene in aqueous media by hydroxyl radicals. J Photochem Photobiol A Chem 215:59–68. https://doi.org/10.1016/j.jphotochem.2010.07.021
40. Hammond GS (1955) A correlation of reaction rates. J Am Chem Soc 77:334–338. https://doi.org/10.1021/ja01607a027
41. Serna-Galvis EA, Silva-Agredo J, Giraldo AL, Flórez OA, Torres-Palma RA (2016) Comparison of route, mechanism and extent of treatment for the degradation of a β-lactam antibiotic by TiO2 photocatalysis, sonochemistry, electrochemistry and the photo-Fenton system. Chem Eng J 284:953–962. https://doi.org/10.1016/j.cej.2015.08.154
42. Timm A, Borowska E, Majewsky M, Merel S, Zwiener C, Bräse S, Horn H (2019) Photolysis of four β-lactam antibiotics under simulated environmental conditions: degradation, transformation products and antibacterial activity. Sci Total Environ 651:1605–1612. https://doi.org/10.1016/j.scitotenv.2018.09.248
43. Antonin VS, Aquino JM, Silva BF, Silva AJ, Rocha-Filho RC (2019) Comparative study on the degradation of cephalexin by four electrochemical advanced oxidation processes: evolution of oxidation intermediates and antimicrobial activity. Chem Eng J 372:1104–1112. https://doi.org/10.1016/j.cej.2019.04.185
44. Song W, Chen W, Cooper WJ, Greaves J, Miller GE (2008) Free-radical destruction of β-lactam antibiotics in aqueous solution. J Phys Chem A 112:7411–7417. https://doi.org/10.1021/jp803229a
45. Ali MA, Rajakumar B (2011) Thermodynamic and kinetic studies of hydroxyl radical reaction with bromine oxide using density functional theory. Comput Theor Chem 964:283–290. https://doi.org/10.1016/j.comptc.2011.01.013

46. Duarte F, Åqvist J, Williams NH, Kamerlin SCL (2015) Resolving apparent conflicts between theoretical and experimental models of phosphate monoester hydrolysis. J Am Chem Soc 137:1081–1093. https://doi.org/10.1021/ja5082712
47. Homem V, Santos L (2011) Degradation and removal methods of antibiotics from aqueous matrices — a review. J Environ Manage 92:2304–2347
48. Giraldo-Aguirre AL, Serna-Galvis EA, Erazo-Erazo ED, Silva-Agredo J, Giraldo-Ospina H, Flórez-Acosta OA, Torres-Palma RA (2018) Removal of β-lactam antibiotics from pharmaceutical wastewaters using photo-Fenton process at near-neutral pH. Environ Sci Pollut Res 25:20293–20303. https://doi.org/10.1007/s11356-017-8420-z
49. Serna-Galvis EA, Montoya-Rodríguez D, Isaza-Pineda L, Ibáñez M, Hernández F, Moncayo-Lasso A, Torres-Palma RA (2019) Sonochemical degradation of antibiotics from representative classes—considerations on structural effects, initial transformation products, antimicrobial activity and matrix. Ultrason Sonochem 50:157–165. https://doi.org/10.1016/j.ultsonch.2018.09.012